JOURNAL OF MAGNETIC RESONANCE **135,** 435–443 (1998)
ARTICLE NO. MN981600

Molecular Diffusion and DNP Enhancement in Aqueous Char Suspensions

B. M. Odintsov,*,‡,§,¶,[1] R. L. Belford,*,† P. J. Ceroke,*,‡ Z. Sh. Idiyatullin,§ R. S. Kashaev,§ I. V. Kuriashkin,*,‡ V. S. Rukhlov,¶ A. N. Temnikov,§ and R. B. Clarkson*,‡,[1]

*Illinois Research EPR Center, †Department of Chemistry, and ‡Department of Veterinary Clinical Medicine, University of Illinois, 190 MSB, 506 S. Mathews, Urbana, Illinois 61801; and §State Technological University and ¶Zavoiski Physical-Technical Institute, Russian Academy of Sciences, Kazan, 420029, Russia

Received February 4, 1998; revised September 9, 1998

The heterogeneous ^{1}H dynamic nuclear polarization (DNP) effect is studied at low magnetic fields for a system consisting of several newly synthesized carbon chars suspended in water. By using Fourier Transform pulsed-field-gradient spin–echo NMR spectroscopy, several different self-diffusion coefficients have been observed in aqueous char suspensions, corresponding to regions of differing water mobility in the porous structure. Proton spin–lattice relaxation data generally confirm the results of molecular diffusion measurements. Through utilization of the Torrey model, the influence of "cage effects" on DNP enhancement in porous media is discussed. Results suggest that short-range nuclear–electronic interactions in pores have a dominant effect on DNP enhancement in char suspensions.

Key Words: **surface–liquid interactions; DNP; NMR.**

INTRODUCTION

An understanding of molecular motion and spin dynamics in porous structures is of central importance to research concerning heterogeneous catalysis, fluid penetration of engineering plastics and ceramics, and biological perfusion. Because of the confining influence of pore boundaries on molecular motion, this motion contains a signature characteristic of pore morphology. Studies of molecular diffusion and relaxation processes in paramagnetic porous materials provide valuable information about surface relaxivity and spin dynamics at the solid–liquid interface (*1–3*).

Over the past two decades, many different magnetic resonance methods have been used in studies of paramagnetic centers in carbonaceous solids as well as in studies of the surface diffusion of solvents adsorbed on charcoals (*2–8*). By means of an EPR technique, it was established that the unpaired electrons responsible for the electron paramagnetism of chars presumably represent stable free organic radicals created during the heat-treatment carbonization procedure. Surface diffusion of different solvents adsorbed on charcoals has already been the subject of NMR relaxation studies (*4–6*). An NMR chemical shift technique also has been applied to study the molecules adsorbed on charcoal and silica gel (*7, 8*). Recently, self-diffusion coefficients in porous media by different kinds of pulsed-field-gradient (PFG) NMR have been the object of intensive theoretical and experimental studies (*9–13*). In spite of significant progress in these studies, the electronic structure of char paramagnetic centers and the process of free radical formation during carbonization, as well as the nature of hyperfine interactions on the surface of chars, are not yet fully understood.

During the past few years there has been a new interest in paramagnetic carbon systems for biomedical applications (*14*). Recently (*15, 16*) we demonstrated the possibility of using char microparticles as a new type of contrast agent in dynamic nuclear polarization (DNP) imaging and DNP oximetry. The efficiency of these contrast agents is determined mainly by the magnitude of the DNP enhancement in polarized nuclei.

The use of the nuclear–electron Overhauser effect to polarize nuclei in both liquids and solids via DNP is a well-known phenomenon (*17*). Studies of DNP already have demonstrated the possibility of obtaining detailed information on the character of intermolecular hyperfine interactions and molecular motion in both liquids and solids (*17–20*). DNP is especially effective when other methods of detecting very weak scalar intermolecular coupling, such as direct observation of hyperfine structure in EPR and chemical shift measurements in NMR, are ineffective due to line broadening (*21*).

In general, the unpaired electron spins used to dynamically polarize the nuclei are distributed uniformly throughout the bulk of the sample. In several cases, DNP can be produced in a liquid by pumping with microwave radiation in resonance with paramagnetic centers near the solid–liquid interface (*20*). There are only a few reported experimental studies of solid–liquid DNP transfer between sublevels in magnetic spin systems consisting of species with different gyromagnetic ratios (*22, 23*). Most of these have described the dominant "solid-state" DNP effect due to pure dipole–dipole intermolecular

[1] To whom correspondence should be addressed. Fax: (217) 333-8868. E-mail: bodintso@uiuc.edu; clarkson@uiuc.edu.

1090-7807/98 $25.00

interactions, such as those observed between free radical labels immobilized on a surface and solvent protons (*22*).

We recently reported (*24*) the first observation of solid–liquid electron spin density transfer in an aqueous system consisting of hardwood chars suspended in water by using an ^{1}H pulsed DNP technique at a low magnetic field. Proton DNP enhancement has been seen for aqueous suspensions of several newly synthesized types of chars, where both positive and negative Overhauser effects were detected in different samples (*24–26*). The magnitudes of the observed NMR absorption as well as emission of water protons in different char suspensions are an order of magnitude less than the theoretical maximum for pure scalar and pure dipolar coupling, respectively. Possible reasons for this lower DNP enhancement can be found in the details of molecular diffusion and spin dynamics in paramagnetic porous media. In this work we experimentally analyze the heterogeneous DNP effect in several chars suspended in water by using several magnetic resonance techniques.

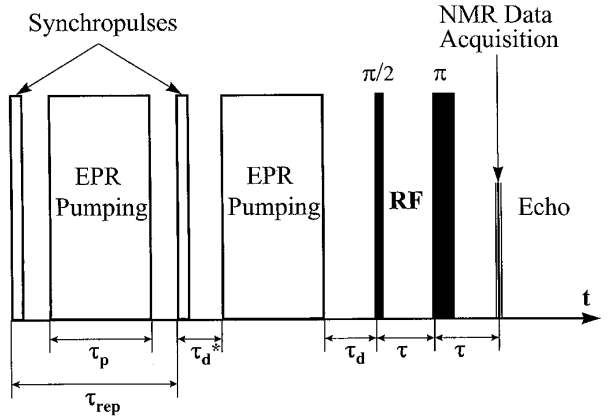

FIG. 1. Time sequence of EPR and NMR pulses in a low-field DNP experiment, where the EPR saturation, NMR pulses, and signal acquisition period are separated in time.

EXPERIMENTAL

Pulsed DNP at Low Magnetic Field

In contrast to traditional NMR and EPR spectroscopy, where chemical (structural) utility is improved at high magnetic fields due to the increase of resolution in the spectrum with frequency, the effectiveness of relaxation phenomena, such as DNP, has a more complicated field dependence (*17–20*). Low magnetic fields are of special interest in liquid and multiple-phase DNP applications, because it is in such fields that cross-relaxation spectral density functions have the highest values. DNP often is able to look at the intermolecular events that bring about the coupling between electron and nuclear spins, and can examine the structural and motion features that govern the interaction. For this purpose, lower magnetic fields, or a range of fields at which data can be obtained, provide the richest information.

The measurements of DNP enhancements of water protons in char suspensions were carried out under the following conditions: $\nu_I = \omega_I/2\pi = 0.5$ MHz, $B_0 = 117.5$ G; the electron resonance frequency was $\nu_S = 328.8$ MHz. A portable NMR relaxometer (*27*) was modified and used to detect the polarized NMR signal. A synchronizing pulse from the NMR relaxometer (Fig. 1) activates the delay generator, which provides the delay time between the EPR-pumping pulse and NMR pulse sequences. At the same time, the delay generator creates a rectangular pulse that modulates the amplitude of a Hewlett–Packard 8647A signal generator, which is the source of the EPR resonance frequency. This RF pulse is then amplified by a Henry Radio power amplifier. A spiral delay line (helix) was used to enhance the EPR saturating field. A two-channel Hewlett–Packard 54600A digital oscilloscope was used to provide display and averaging of the NMR signal amplitude (channel 1) and for measurement of the voltage on a high-frequency diode (channel 2), which is proportional to the EPR saturation field amplitude, B_{1S}, inside the EPR helix. The proportionality coefficient between the voltage and B_{1S} was determined in separate experiments with a 1 mM aqueous solution of Fremy's salt $K_2[NO(SO_3)_2]$ of known electronic relaxation times (*21*). We used the pulse sequence described in Fig. 1, where the EPR saturating pulse, NMR pulse sequence, and signal acquisition period were separated in time. The period of the EPR saturating pulses can be chosen to avoid microwave heating of the sample. Details of the experimental apparatus are described elsewhere (*21*).

Following Solomon (*28*), one can determine a quantitative expression for the time dependence of NMR magnetization $\langle I_z \rangle$ in coupled nuclear–electron system

$$d\langle I_z\rangle/dt = -[(\langle I_z\rangle - I_0) + \xi f(\langle S_z\rangle - S_0)]/T_{1n}, \qquad [1]$$

where ξ is the nuclear–electron coupling parameter. I_0 and S_0 represent the equilibrium nuclear and electronic magnetization, respectively. The leakage factor for nuclear spins in homogeneous solutions of paramagnetic ions and free radicals is usually calculated by the formula (*17*)

$$f = 1 - T_1/T_1(0), \qquad [2]$$

where T_1 and $T_1(0)$ are the experimentally obtained nuclear spin–lattice relaxation times in a solution and pure solvent, respectively.

For many systems, it can be assumed that on the scale of nuclear relaxation times, electronic relaxation happens instantly. This assumption gives us the initial conditions for the integration of Eq. [1]. For a two-pulse Hahn NMR sequence generated after an EPR pumping pulse, the master equation describing the relative amplitude enhancement A of the nuclear

TABLE 1
Experimental DNP Data in Aqueous Chars Suspensions at Magnetic Field 117.5 G

N	Material	T_1^{av}(s)		A_{max}	
1	Hardwood	0.28	0.01	+20	0.3
2	Starch	0.31	0.01	−24	0.3
3	Fructose	0.49	0.02	−65	2.1

spin echo signal V derived from a polarized sample can be obtained from [1],

$$A = [V - V_0]/V_0 = A_{max} Z[1 - \exp(-\tau_p/T_1)]\exp(-\tau_d/T_1), \quad [3]$$

where V_0 is the amplitude of the nonpolarized echo, τ_p is the duration of the EPR saturation pulse, and τ_d is the delay time between EPR and $\pi/2$ NMR pulses (see Fig. 1). Parameter A_{max} is defined as

$$A_{max} = -\xi f \gamma_s/\gamma_I, \quad [4]$$

where $|\gamma_s/\gamma_I| = 660$ for protons.

The value $Z = (S_0 - \langle S_z \rangle)/S_0$ in [3] is the EPR saturation parameter, which depends on the EPR line shape. For the simplest case of a single Lorentzian EPR line, saturated in the center,

$$Z = \gamma_s^2 B_{1S}^2 \tau_S^2/(1 + \gamma_s^2 B_{1S}^2 \tau_S^2), \quad [5]$$

where $\tau_S = (T_{1S}T_{2S})^{1/2}$. In this case, the reciprocal value of the NMR enhancement, A^{-1}, depends linearly upon the square of the reciprocal of the EPR saturating field amplitude, B_{1S}^{-2}. The slope of the graph of this dependence is determined by the product of electron relaxation times $T_{1S}T_{2S}$. In the case of an inhomogeneous EPR line, this dependence becomes more complicated (*16*). Note that there are no adjustable parameters in expressions [2]–[5].

Parameters A_{max} and ξ in [3] were found experimentally by extrapolating a plot of $A^{-1}[1 - \exp(-\tau_p/T_{1n})]\exp(-\tau_d/T_{1n})$ vs B_{1S}^{-2} to zero of B_{1S}^{-2} according to Eq. [5]. The leakage factor, f, was obtained by measuring T_1 and $T_1(0)$ by formula [2]. According to [3], the spin–lattice relaxation time T_1 can be measured in two ways—by changing either the polarization time τ_p or the delay time τ_d between the EPR pulse and the NMR pulse sequence. Both methods were utilized in these experiments. It should be emphasized that in low-field DNP experiments, the volumetrically averaged DNP parameters usually are measured, as is shown in Table 1. The major source of error in the DNP/NMR experiment at low magnetic fields arises from the inaccuracy in measuring the nonpolarized NMR signal intensity, V_0; by utilizing the averaging options of a HP 54600A oscilloscope, the relative experimental error was decreased to 5%.

Pulsed-Field-Gradient Spin–Echo NMR Spectroscopy

PFG NMR has attracted renewed attention as a probe of microscopic but volumetrically averaged properties of materials (*10–13*). This method is one of the best tools for measuring the time-dependent diffusion coefficient (*10*). The measurement is nondestructive and does not involve the introduction of chemical or isotopic tracers (*11*). The theoretical foundation of this method is based on the dependence of the spin–echo amplitude on the external magnetic field gradient value g (*29–32*). The quantitative relationship between spin–echo amplitude attenuation and self-diffusion coefficient D is given by the well-known equation (*11*)

$$\ln(A_G/A_0) = -k^2 t_{diff} D, \quad [6]$$

where A_G is the spin–echo signal amplitude and A_0 is the amplitude with no gradients, $k = \gamma g \delta$, where γ is the gyromagnetic ratio of the nucleus, δ is the gradient pulse duration, and the diffusion time, $t_{diff} = (\tau - \delta/3)$, is a function of the duration of the applied gradient as well as the separation between the diffusion-sensitive gradient pair, τ. Equation [6] gives us the possibility to determine the self-diffusion coefficient D by changing g, δ, or τ values, because the molecular diffusion process causes a proportional decrease of the spin–echo signal amplitude. If a series of experiments are performed where only g is varied incrementally, then the slope of a linear plot of $\ln(A_G/A_0)$ vs $k^2 t_{diff}$ can be used to calculate the self-diffusion coefficient, D, for freely diffusing molecules. Thus in a simple monocomponent dilute solution, a plot of $\ln(A_G/A_0)$ vs k^2 is a straight line. The slope of the graph of this dependence is determined by the self-diffusion coefficient. When several different types of molecules with different self-diffusion coefficients are present in solution, the data often can be deconvoluted by means of multicomponent mixture analysis, resulting in values of D^i for each component in the system. In this case the function $\ln(A_G/A_0)$ is a combination of several lines with the slopes determined by the corresponding diffusion coefficients (*13*). One can use traditional graphical analysis, with consecutive subtraction of diffusive components from the total curve, to determine each D^i present in the data.

The measurement of self-diffusion coefficients of water molecules in char suspensions was performed at room temperature with a modified Tesla-BS-567A high-resolution NMR spectrometer operated at a Larmor ^{1}H frequency of 100 MHz and equipped with a Fourier transform accessory. The spectrometer was modified with two self-shielded gradient Helmholtz coils that can achieve a maximum gradient strength of 50 G/cm. We used the pulse sequence described in Fig. 2, where the gradients are turned off during the RF pulses and the signal acquisition period. The standard relaxation Hahn pulse sequence

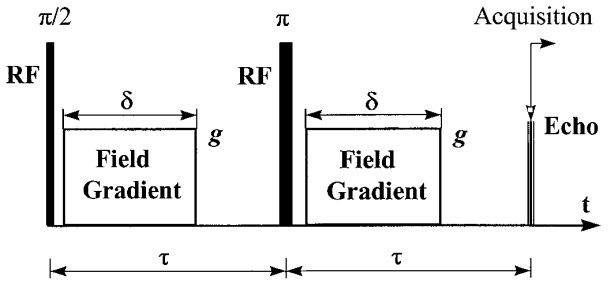

FIG. 2. The pulsed-field-gradient spin–echo pulse sequence used to measure diffusion in char suspensions. In our experiments, $\delta = 8$ ms and $\tau = 30$ ms, and the strength of applied gradient g pulse was varied as explained in the text.

program was modified to introduce the gradient pulses as well as a delay τ between the end of the second RF pulse and the start of data accumulation, the delay being equal to the time between the two of pulses as shown in Fig. 2. The right half of the spin–echo signal was Fourier transformed and analyzed. The FT-PFG NMR technique allows one to increase the measurement accuracy (*11*). Experiments were performed by varying the gradient strength g and keeping the gradient width δ and all other timing parameters constant. Typically the values $\delta = 8$ ms and $\tau = 30$ ms were used for the width of the gradient pulse and time interval between Hahn $\pi/2$ and π RF pulses, respectively. It should be noted that only diffusion components which are not completely relaxed within the time interval 2τ can be analyzed. Experimental error of self-diffusion measurements did not exceed 5%.

NMR Relaxometry

Spin–lattice relaxation times T_1^i of water protons in char suspensions were measured by an NMR relaxometer NMR-07PC, which is a modification of the previous model described in (*33*). Special software has been created to account for multi-exponential relaxation, in which the relaxation (echo–decay) curve was described as a sum of several components $A(t)/A(0) = P_i F_i(t)$ with the corresponding weighting coefficients P_i. The exponential form of each component $F_i(t) = \exp(-t/T_1)$ was used. To avoid the possible influence of slightly nonexponential time dependencies of $F_i(t)$, only the initial part of each component was used, with the consecutive subtraction of the most slowly relaxing $F_i(t)$-components from the total curve. Relaxation times and relative intensities P_i of each component were determined by linear least squares analysis. The dynamic range of the relaxation measurement followed the decay of the echo out to 1/50 of its initial amplitude. Experiments were carried out at room temperature at a proton resonance frequency of 6 MHz. The pulse sequence ($\pi/2$–τ–π /2–τ–π) was used. Data were averaged over 50 acquisitions with a recycling delay of 10 s to avoid saturation. Experimental error of relaxation time measurements did not exceed 5%.

Samples

Samples of chars used in this work were produced by a thermal treatment of carbonaceous materials, obtained from various kinds of woods (e.g., hardwoods, softwoods), starch, and fructose, by charring under an H_2 and CH_4 flow. Not only do the properties of chars depend upon the nature of the starting material, they also are strongly affected by thermal treatment (both the temperatures and the times of heating) and the gas atmosphere in which the thermal treatment is carried out. The samples were heated at the rate of 10°C/h according to a preselected heat-treatment profile, with a maximum temperature ranging from 420 to 720°C. Preparation techniques included digitally programmed temperature profiles, ball milling, and size separation by microsieving. A particle size of about 450 μm was used in these experiments. The samples were suspended in water and then bubbled with pure helium for 15 min to reduce the concentration of dissolved oxygen in the solvent. A concentration of 0.64 g/cm^3 of char suspended in water was used. The EPR spectra of chars in water at room temperature consisted of single, nearly Lorenzian lines, with peak-to-peak line widths of about 1.0 G, and a typical free radical g-factor close to the free electron value of 2.0023. Experimental details of char synthesis are described elsewhere (*16, 34*).

RESULTS AND DISCUSSION

In this study, the proton DNP enhancement of water molecules was observed in aqueous suspensions of several newly synthesized types of chars, where both positive and negative Overhauser effects were detected in different samples. Table 1 shows DNP parameters and proton spin–lattice relaxation times T_1 for chars suspended in water with different nuclear–electron interactions. Negative DNP enhancement was observed in fructose char suspensions as a result of the dominant dipolar–dipolar (through space) hyperfine interactions at the solid–liquid interface. Positive DNP enhancement was observed in several hardwood char suspensions, which is strong evidence for a short-range contact hyperfine interaction at the solid–liquid interface (*17–20*). This coupling leads to electron delocalization from paramagnetic centers on the char surface to water protons in the solvent, since the contact interaction demands that there be a nonzero value for the electronic wave function at the nucleus (*17*). In accordance with (*2*) and (*3*), the linear dependence of positive DNP enhancement A^{-1} on B_{1s-2} was observed in hardwood char suspensions (Fig. 3a), indicating the homogeneous nature of EPR line broadening in the chars. Good linearity also was observed in samples that demonstrated a negative enhancement (Fig. 3b).

A strong temperature dependence of the DNP enhancement was observed in aqueous suspensions of hardwood chars (Fig. 4a). With increasing temperature, the sign of the water proton DNP enhancement in several hardwood char suspensions

changed (Fig. 4b) from negative (NMR emission of polarized proton signal) to positive (NMR absorption), indicating a change in the relative contributions from exchange (scalar) and dipole–dipole nuclear–electron coupling (*25*). The increase in scalar polarization with temperature suggests the possibility of exchange processes at the solid–liquid interface. A model of molecular migration at the solid–liquid interface was constructed in our work (*25*) to account for these observations. Correlation of experimental and theoretical results has been achieved through consideration of the proton–electron spin dipole–dipole interaction and of chemical exchange of solvent molecules.

In contrast to hardwood chars, the negative DNP enhancement in fructose char suspensions was practically temperature independent (Fig. 4c), suggesting that the frequency dispersion (*17–20*) is negligible in these systems and the "white spectrum" condition is realized in the frequency region under investigation. The temperature independence of the DNP enhancement in fructose char suspensions also reflects the dominant dipole–dipole type of hyperfine interaction at the solid–liquid interface, since the change in temperature does not lead to a change in the balance between dipole–dipole and scalar solid–liquid interactions, as in the case of hardwood char suspensions (Figs. 4a and 4b).

A DNP control experiment was run in which the char particles were filtered out of the water solution. No DNP enhancement was detected in the filtered water. This indicates that the chars were not dissolving and that no solvated molecules were giving rise to DNP. Only solid–liquid hyperfine interactions with water, chemisorbed on the large char particles containing unpaired electrons, are important and give rise to DNP effect in these systems.

The magnitudes of the observed positive and negative DNP enhancements in char suspensions (Table 1) are an order of magnitude less than the theoretical maximum of pure scalar +330 (scalar relaxation of Abragam's Type II) and pure dipolar −330 coupling, respectively. One possible reason for this lower enhancement is a delicate balance between dipole–dipole and scalar solid–liquid interactions in these systems. The importance of this mechanism was analyzed in our work (*25*). It was shown that the effectiveness of this mechanism critically depends on temperature. However, the change in temperature in fructose char suspensions does not lead to a change in the balance between dipole–dipole and scalar solid–liquid interactions, as in the case of hardwood char suspensions (Fig. 4c).

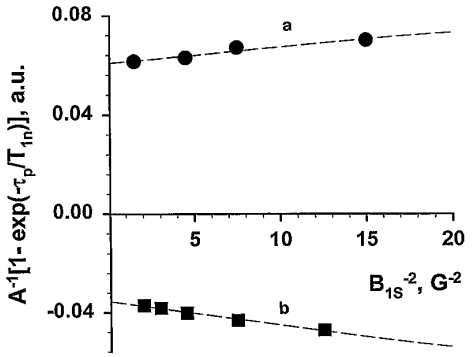

FIG. 3. Plots of experimental EPR saturation for hardwood (a) and fructose (b) chars suspended in water at $T = 300$°K. From best straight lines fitted to the data, the A_{max} values have been found (Table 1).

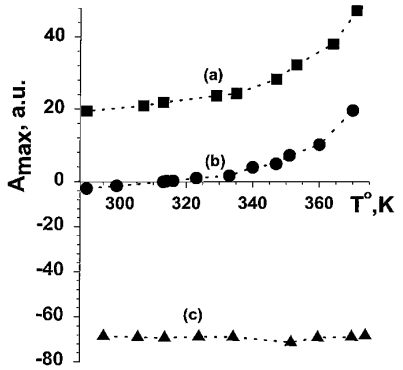

FIG. 4. Temperature dependence of DNP enhancements of water protons in an aqueous suspensions of chars with different initial charring materials (atmosphere of charring): (a) hardwood (H_2), (b) hardwood (CH_4), and (c) fructose (H_2) at $B_{1S} = 0$, 1 G, $\tau_p = 0.5$ s, $\tau_d = 4$ ms.

Another important mechanism is the possible influence on the value of DNP enhancement of a gradual transition from the pure "liquid" DNP effect to the pure "solid-state" effect at ($\omega_s \pm \omega_I$). One expects to find this transition when the correlation time of liquid motion goes from values much shorter to values much longer than the transverse electron relaxation time T_{2S}, although more detailed criteria (*36–38*) also involve T_{1S}. Heisenberg electron–electron spin exchange at the surface of chars, where the concentration of paramagnetic centers is high, can be considered as a modulation mechanism (in addition to thermal molecular motion) for DNP phenomenon at the solid–liquid interface and may affect the DNP enhancement in char suspensions. The intensity of electron spin exchange can influence the gradual transition from the pure "liquid" DNP effect to the pure "solid effect" in such paramagnetic multiple-phase systems. The maximum value of polarization in the intermediate situation lacks the symmetry in $\Delta\omega$ of the "liquid" effects ($\Delta\omega = 0$) (*17*). However, in all investigated compounds the maximum DNP enhancement was achieved with the microwave frequency centered on the EPR line, indicating that the dynamic polarization occurs through the Overhauser mechanism, as opposed to "solid-state" effect (*17, 18, 35*).

The self-diffusion coefficients D for aqueous char suspensions have been measured by using the FT-PFG NMR technique. Typical raw PFG data are shown in Fig. 5. The near-linear dependence of $\ln(A_g/A_0)$ on the gradient strength g was observed in fructose char suspensions. This is an important feature of the data, as it indicates that the water molecules are largely undergoing unbounded diffusion in this kind of char system. This observation may be the result of the hydrophobic

character of fructose char surfaces, which would favor fast translational diffusion, with high D values, for water near the solid–liquid interface. The low porosity of fructose chars also may contribute to the effect. It should be noted that the hydrophobic character of fructose char is in good agreement with the dominant dipole–dipole (through space) type of solid–liquid hyperfine interactions which leads to negative DNP enhancement in these char suspensions (Table 1).

In contrast to fructose char suspensions, the data obtained from hardwood chars show the effects of pores on the PFG-NMR diffusion measurements, as seen in Fig. 5. The observation suggests the hydrophilic character of these chars surface with developed porous structure. Hydrophilic character would promote the short-distance contact hyperfine coupling at the solid–liquid interface, which leads to electron delocalization from paramagnetic centers on the char surface to water protons and to positive DNP enhancement in hardwood char suspensions (Table 1). The maximum $D^0 = 2 \times 10^{-5}$ cm^2/s value obtained in all investigated compounds correlates with the diffusion coefficient in pure water at 30°C ($D = 2.55 \times 10^{-5}$ cm^2/s) and can be attributed to the molecules in bulk water (volume V^0 in Fig. 6). A minimum $D^s = 0.06 \times 10^{-5}$ cm^2/s value was observed in hardwood char suspensions (Table 2), which indicates strong bonding of water molecules with the surface of chars and can be attributed to the fluid molecules in the remainder of the surface layer (volume V^S in Fig. 6) with a mobility less than 1/30 that of molecules in bulk water.

Proton spin–lattice relaxation data generally confirm the results of molecular diffusion measurements. The longest T_1^0 (1 s) can be attributed to the relaxation time of the "bulk" water (volume V^0 in Fig. 6) and corresponds to the high molecular mobility in this area with maximum diffusion coefficient D^0 (Table 2). Middle values for T_1^s (0.3–0.4 s) can be attributed to

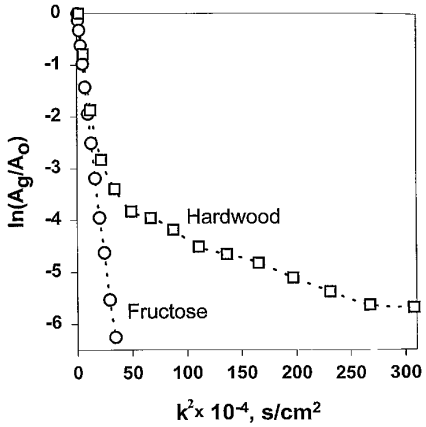

FIG. 5. Typical raw PFG-NMR data. Plot of $\ln(A_G/A_0)$ vs $k = \gamma g \delta$, for different chars saturated with water. The squares are data obtained from water diffusing in hardwood char suspensions and clearly illustrate the effects of restriction on the PFG-NMR diffusion experiment. The circles are data taken from water in fructose suspensions under the same experimental conditions and represents the curve for unrestricted diffusion.

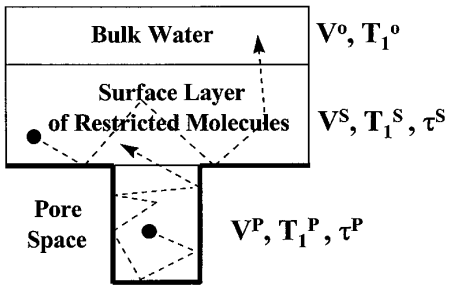

FIG. 6. Schematic illustrating the effect of restricting boundaries on water diffusion and relaxation measurements in char suspensions.

the envelope of water molecules (volume V^S in Fig. 6) having contact with the "bulk" water and exhibiting diffusion coefficient D^S. The shortest relaxation times T_1^p (30–50 ms) correspond to the water molecules in the vicinity of paramagnetic centers mainly in pore space (volume V^P in Fig. 6), where they strongly interact with the free radicals on the surface of the char and undergo multiple collisions with the paramagnetic walls in a porous cage.

Unbounded molecular diffusion in fructose char suspensions leads to fast molecular motion near the surface–liquid interface, which results in a long relaxation time. Intensive molecular motion initiates fast exchange between "surface" and "bulk" water and gives us the averaged relaxation time $T_1^0 = T_1^S = 1.2$ s (Table 2), which is comparable to T_1 in pure water. Analyzing the results of Table 2, one can find that in hardwood char suspensions the fraction of water molecules in pore space is equal to 8.2% as compared to only 2% in fructose char, suggesting an essential difference in the porous structure of these chars.

Following Torrey (*39*), let an amount of fluid with volume V be bounded by a porous solid (Fig. 6). The surface of the solid contains a number of paramagnetic centers which are in resonance with a microwave power source. We denote by V^p the volume occupied by fluid molecules in pores in the immediate vicinity of these centers and by V^S (which is part of V) the volume occupied by fluid molecules in the remainder of the surface layer. The nuclei in V^p as well as in V^S are flipped at a given rate by the external microwave power through the Overhauser effect with the characteristic relaxation times T_1^p and T_1^S, respectively. Some flipped nuclei escape to the volume V^0 before they are relaxed, where they are exposed to ordinary relaxation, characterized by the relaxation time T_1^0.

The following equation has been derived (*38*) for the experimentally observed (volumetrically average) spin–lattice relaxation time T_1^{av} of the fluid in the porous media:

$$(T_1^{av})^{-1} = (T_1^0)^{-1} + (V^S/V)/(T_1^S + \tau^S) + (V^p/V)/(T_1^p + \tau^p); \quad [7]$$

here τ^S and τ^p are the residence times of molecules entering V^S

TABLE 2
Self-Diffusion Coefficients and NMR Relaxation Data in Aqueous Char Suspensions

N	Material	$D^0 \times 10^5$ (cm^2/s)	$D^s \times 10^5$ (cm^2/s)	V^0 (%)	V^s (%)	V^p (%)	T_1^0 (s)	T_1^s (s)	T_1^P (s)
1	Hardwood	1.6	0.06	7.8	84	8.2	0.9	0.32	0.033
		0.2	0.006	0.4	2	0.4	0.06	0.02	0.02
2	Starch	1.75	0.1	7.9	89	3.1	1.02	0.35	0.048
		0.2	0.01	0.4	2	0.6	0.06	0.02	0.02
3	Fructose	1.96	0.2	98	2	2.0	1.2	0.06	0.04
						0.2			0.001

and V^P, respectively. Through use of the equation for nuclear relaxation with diffusion (*39*), the following formula was obtained in (*38*) for the nuclear leakage factor f in porous media:

$$f = [1 + V^S(T_1^P + \tau^p)/V^p(T_1^S + \tau^S) + (T_1^P + \tau^p)/V^pT_1^0]^{-1}; \quad [8]$$

here we assumed $V = 1$. In the case of $T_1^P \ll T_1^0$ the leakage factor f, as well as the DNP enhancement, depends mainly on the relative efficiency of proton relaxation in volumes V^s and V^P:

$$f = [1 + V^S(T_1^P + \tau^p)/V^P(T_1^S + \tau^S)]^{-1}. \quad [9]$$

Thus one obtains the full Overhauser effect if the relaxation in V^P dominates and the inequality

$$V^s/(T_1^S + \tau^S) \ll V^p/(T_1^P + \tau^p) \quad [10]$$

is satisfied. If relaxation in V^S dominates, one finds a reduced effect. Figure 7 shows the dependence of the DNP enhancement value A on the efficiency of proton relaxation in the two different zones V^S and V^p for a fructose char suspension in accordance with Eqs. [3] and [8].

Using Eqs. [7]–[8] one can estimate the residence times of water molecules in pore space V^P according to the formula

$$\tau^p = V^pT_1^{av}/f - T_1^P$$
$$\tau^S = V^ST_1^{av}T_1^0/[T_1^0(1 - f) - T_1^{av}] - T_1^S. \quad [11]$$

Assume that the pure dipole–dipole type of hyperfine interaction is present in fructose char suspensions and that the nuclear–electron coupling parameter ξ in [4] is equal to its theoretical value $\xi = +0.5$. Then, the lower-than-expected experimental value of the DNP enhancement can be understood theoretically by a smaller leakage factor in porous media. Using DNP and relaxation data from Tables 1 and 2, and calculating the leakage factor value as $f_{theor} = A_{max}/330 = 0.2$, one can estimate from [11] the residence times in the V^P and V^S zones. Calculations give $\tau^p = 9$ ms and $\tau^S = 24$ ms for fructose char suspensions.

Figure 8 shows the dependence of the leakage factor f on the residence times τ^p and τ^S in fructose char suspensions. It follows from Fig. 8 that the f value (and as a result the value of DNP enhancement) in char suspensions depends mainly on the residence time τ^p of water molecules in pore space. Increasing τ^p leads to a decrease of the DNP effect in porous media. In other words, if the exchange of water

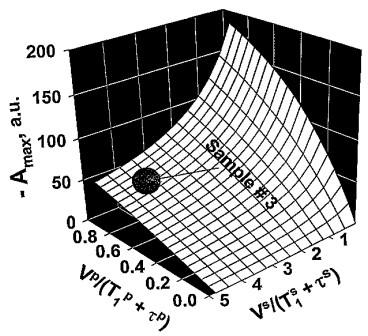

FIG. 7. The dependence of DNP enhancement value A on the efficiency of proton relaxation in two different zones V^S and V^p for fructose char suspensions.

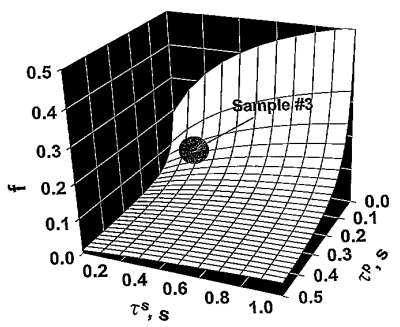

FIG. 8. The dependence of leakage factor f on the sticking time values of τ^p and τ^S for fructose char suspensions.

molecules between V^P and V^S zones is blocked and the inequality

$$\tau^p > V^p(T_1^S + \tau^S)/V^S - T_1^p \qquad [12]$$

is satisfied, one obtains a reduced DNP effect in accordance with Eq. [10]. This "cage effect" obviously will increase with increasing tortuosity of the pore structure. On the other hand, increasing the pore volume V^P, leads to an increased leakage factor and larger DNP effect in char suspensions (Fig. 9). Relaxation processes in the pore space (T_1^P) and in the remainder of the surface layer (T_1^S) have an opposite influence on DNP enhancement (Fig. 10). A decrease of the relaxation time T_1^P in the porous space is the main influence responsible for the increase of the DNP effect. At the same time, shorter T_1^P allows one to use a shorter EPR saturation pulse in DNP experiments, in accordance with Eq. [3].

CONCLUSIONS

The main DNP processes in char suspensions occur in pores, and the short-range nuclear–electronic interactions in pores have a dominant effect on DNP enhancement. Long-range interactions associated with other (nuclear and electron–nuclear) relaxation processes at the remainder of the surface layer have a small or even negligible effect. As a result, the value of the DNP enhancement in char suspensions will increase under the following conditions:

1. with a decrease of the pore size and tortuosity of pore structure, which leads to a decrease of the residence time τ^P in the pore space, and as a result, to more intensive exchange of strongly polarized nuclei in pores with nuclei in the bulk solvent;

2. with increase in pore volume V^P, compared with the volume V^S in the remainder of the surface layer;

3. with a decrease in the spin–lattice relaxation time T_1^P in the pore space; it should be noted that the shortening of T_1^P allows the use of a shorter EPR saturation pulse in DNP experiments (τ_p in Eq. [3]), which is especially important in conducting materials to avoid the microwave heating of the sample.

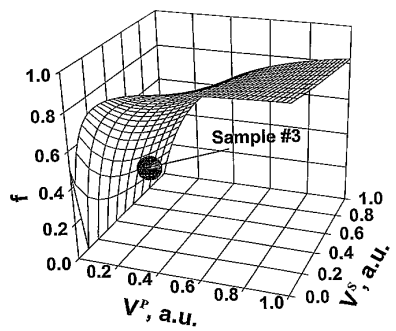

FIG. 9. The dependence of leakage factor f on the volumes V^P and V^S of pore space and in the remainder of the surface layer, respectively in fructose char suspensions.

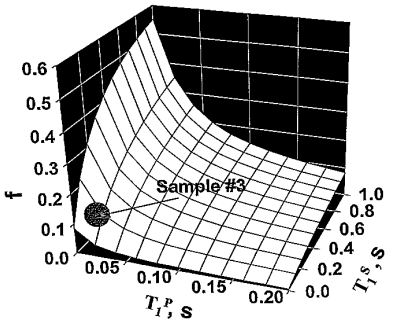

FIG. 10. Influence of the nuclear relaxation time values in pore space (T_1^P) and in the remainder of the surface layer (T_1^S) on nuclear leakage factor f in fructose char suspensions.

Thus the synthesis of chars with developed porous structure and small pore size, low tortuosity, and fast spin–lattice relaxation in the pore space leads to an increase of the DNP effect in char suspensions.

In spite of the good agreement between this model and our experimental data, there still remains a question regarding the possibility that differences in surface chemistry between chars of the different composition could account for some of the effects we attribute to porosity. In a previous study (*25*), we measured the values of E_h, the Arrhenius activation energy for water desorption, in hardwood, softwood, and starch chars. This parameter is a direct reflection of the water/char chemistry, and it is nearly identical (± 0.5 kcal/mol) for these systems, suggesting very similar surface chemistry. Yet the softwood and starch chars do not demonstrate the same temperature dependencies for DNP enhancements as does the hardwood char. This observation leads us to state that differences in porosity of the chars must play a critical role in the DNP effect. Of course, surface chemistry also can be important, and future research is aimed at a clearer understanding of the interplay of structure and chemistry in these complex systems.

ACKNOWLEDGMENTS

The research was supported in part by a grant from NATO (HTECH. LG 972264) and from NIH (GM51630 to R.B.C.) as well as from the U.S. Department of Energy (DE FG22-96 PC 96205) and used facilities of the Illinois EPR Research Center (NIH P41-RR01811).

REFERENCES

1. H. L. Retcofsky, M. R. Hough, M. M. Maguire, and R. B. Clarkson, Coal structure, *in* "Advances in Chemistry" (M. L. Golbaty and K. Ouchi, Eds.), pp. 37–53, Am. Chem. Soc., Washington, DC (1981).
2. K. S. Rothenberger, R. F. Sprecher, S. M. Gastellano, and H. L. Retcofsky, Magnetic resonance of carbonaceous solids, *in* "Ad-

vances in Chemistry" (R. B. Botto and Y. Sanada, Eds.), pp. 581–598, Am. Chem. Soc., Washington, DC (1981).

3. F. P. Auteri, R. L. Belford, and R. B. Clarkson, Carbon-based standards for EPR spectroscopy, *Appl. Magn. Reson.* **6,** 287–308 (1994).
4. H. A. Resing, Nuclear magnetic resonance relaxation of molecules adsorbed on surfaces, *Adv. Mol. Relax. Proc.* **1,** 109–154 (1967–1968).
5. J. K. Thompson, J. J. Krebs, and H. A. Resing, NMR relaxation of benzene adsorbed on charcoal: molecular rotation and diffusion, *J. Phys. Chem.* **43,** 3853–3865 (1965).
6. H. A. Resing, J. K. Thompson, and J. J. Krebs, Nuclear magnetic resonance relaxation times of water adsorbed on charcoal, *J. Phys. Chem.* **68,** 1621–1627 (1964).
7. S. Kaplan, H. A. Resing, and A. Waugh, 13C NMR chemical shift anisotropy for benzene adsorbed on charcoal and silica gel, *J. Chem. Phys.* **59,** 5681–5687 (1973).
8. E. G. Derouane, J. Fraissard, J. J. Fripiat, and W. E. E. Stone, NMR studies in adsorption and heterogeneous catalysis, *Catal. Rev.* **7,** 121–138 (1972).
9. P. T. Callaghan, A. Coy, D. MacGowan, K. J. Packer, and F. O. Zelaya, Diffraction-like effects in NMR diffusion studies of fluids in porous solids, *Nature* **351,** 467–469 (1991).
10. B. Antalek and K. Chari, Motion of a polymer chain in surfactant solutions, *Mod. Phys. Lett. B* **9,** 155–159 (1995).
11. C. S. Johnson, Jr., Diffusion measurements by magnetic field gradient methods, *in* "Encyclopedia of NMR" (D. M. Grant and R. K. Harris, Eds.), pp. 1626–1644, Wiley, New York (1996).
12. M. D. Hurlimann, K. G. Helmer, L. L. Latour, and C. H. Sotak, Restricted diffusion in sedimentary rocks, *J. Magn. Reson. A* **111,** 169–178 (1994).
13. R. L. Kleinberg, L. L. Latour, P. P. Mitra, and C. H. Sotak, Pore size distributions and tortuosity in heterogeneous porous media, *J. Magn. Reson.* **112,** 83–91 (1995).
14. H. M. Swartz, S. Boyer, P. Gast, J. F. Glockner, H. Hu, K. J. Liu, M. Moussavi, S.-W. Norby, N. Vahidi, T. Walczak, M. Wu, and R. B. Clarkson, Measurements of pertinent concentrations of oxygen *in vivo, Magn. Reson. Med* **20,** 333–338 (1991).
15. R. B. Clarkson, P. J. Ceroke, and B. M. Odintsov, Carbon chars as oxygen and nitric oxide sensors for biomedical applications, *in* "23rd Biennial Conference on Carbon," Vol. 2, pp. 142–143 (1997).
16. R. B. Clarkson, B. M. Odintsov, P. J. Ceroke, J. H. Ardenkjar-Larsen, M. Fruianu, and R. L. Belford, Electron paramagnetic resonance and DNP of char suspensions: surface science and oximetry, *Phys. Med. Biol.* **43,** 1907–1920 (1998).
17. A. Abragam, "Principles of Nuclear Magnetism," Oxford Univ. Press, Oxford (1961).
18. K. H. Hausser and D. Stehlik, Dynamic nuclear polarization in liquids, *Adv. Magn. Reson.* **3,** 79–146 (1969).
19. J. Potenza, Measurements and applications of DNP, *Adv. Mol. Relax. Proc.* **4,** 229–248 (1972).
20. R. D. Bates, Jr., Dynamic nuclear polarization, *Magn. Reson. Rev.* **16,** 237–291 (1993).
21. B. M. Odintsov, R. L. Belford, and R. B. Clarkson, Cross relaxation in electron–nuclear coupled systems, *J. Phys. Chem.* **101,** 116–120 (1997).
22. H. C. Dorn, T. E. Glass, R. Gitti, and K. H. Tsai, Transfer of ^{1}H and ^{13}C dynamic nuclear polarization from immobilized nitroxide radicals to flowing liquids, *Appl. Magn. Reson.* **2,** 9–27 (1991).
23. G. G. Maresch, R. D. Kendrick, and C. S. Yannoni, Dynamic nuclear polarization via confined electrons in bulk solids, *J. Magn. Reson.* **82,** 41–50 (1989).
24. B. M. Odintsov, R. L. Belford, P. J. Ceroke, and R. B. Clarkson, Solid–liquid electron density transfer in aqueous char suspensions, *J. Am. Chem. Soc.* **120,** 1076–1077 (1998).
25. B. M. Odintsov, R. L. Belford, P. J. Ceroke, and R. B. Clarkson, Temperature dependence of solid-liquid scalar interactions in aqueous char suspensions, *Surf. Sci.* **393,** 162–170 (1997).
26. B. M. Odintsov, R. L. Belford, P. J. Ceroke, and R. B. Clarkson, Low-field DNP studies of solvent molecules at the carbon char/liquid interface *in* "23rd Biennial Conference on Carbon," Penn. State Univ., State College, PA (1997).
27. B. M. Odintsov, Portable NMR relaxometer, *EPR Newsletter* **7,** 29 (1995).
28. I. Solomon, Relaxation processes in a system of two spins, *Phys. Rev.* **99,** 559–562 (1955).
29. E. O. Steijskal and J. E. Tanner, Spin diffusion measurements, *J. Chem. Phys.* **42,** 288–292 (1965).
30. J. E. Tanner and E. O. Steijskal, Restricted self-diffusion of protons in colloidal systems by the pulsed-gradient, spin–echo method, *J. Chem. Phys.* **49,** 1768–1777 (1968).
31. P. Stilbs, Molecular self-diffusion coefficients in Fourier transform nuclear magnetic resonance spectrometric analysis of complex mixtures, *Anal. Chem.* **53,** 2135–2137 (1981).
32. P. Stilbs, Fourier transform pulsed-gradient spin–echo studies of molecular diffusion, *Progr. NMR Spectrosc.* **19,** 1–45 (1987).
33. Z. Sh. Idiatullin, A. N. Temnikov, and R. S. Kashaev, Pulsed NMR spectrometer at 6MHz, *Pribory i Technica Experimenta* **5,** 46–49 (1992).
34. S. Boyer and R. B. Clarkson, Electron paramagnetic resonance studies of an active carbon, *Colloids Surf. A* **82,** 217–220 (1994).
35. E. H. Poindexter, Dynamic nuclear polarization and molecular aggregation in asphaltene suspensions, *J. Colloid Interface Sci.* **38,** 412–423 (1972).
36. P. Papon, J. L. Motchane, and J. Korringa, Unitary theory of dynamic polarization of nuclear spins in liquids and solids, *Phys. Rev.* **175,** 641–649 (1968).
37. J. Leblond, J. Uebersfeld, and J. Korringa, Study of the liquid–state dynamics by means of magnetic resonance and dynamic polarization, *Phys. Rev.* **4,** 1532–1538 (1971).
38. H. C. Torrey, J. Korringa, D. O. Seevers, and J. Ubersfeld, Magnetic spin pumping in liquids contained in porous media, *Phys. Rev. Lett.* **3,** 418–419 (1959).
39. H. C. Torrey, Bloch equation with diffusion terms, *Phys. Rev.* **104,** 563–567 (1956).